Appl. Phys. B 80, 617–625 (2005)
DOI: 10.1007/s00340-005-1764-y

**Applied Physics B**
**Lasers and Optics**

G. WYSOCKI✉
A.A. KOSTEREV
F.K. TITTEL

# Spectroscopic trace-gas sensor with rapidly scanned wavelengths of a pulsed quantum cascade laser for in situ NO monitoring of industrial exhaust systems

Department of Electrical and Computer Engineering, Rice University, 6100 Main Street, Houston, TX 77251, USA

**Received: 30 November 2004 /**
**Revised version: 7 January 2005**
**Published online: 7 March 2005 •** 

**ABSTRACT** Development of a pulsed quantum cascade laser (QCL)-based spectroscopic trace-gas sensor for sub-part-per-million detection of nitric oxide (NO) and capable of monitoring other molecular species such as $CO_2$, $H_2O$, and $NH_3$ in industrial combustion exhaust systems is reported. Rapid frequency modulation is applied to the QCL to minimize the influence of fluctuating non-selective absorption. A novel method utilizes only a few laser pulses within a single wavelength scan to probe an absorption spectrum at precisely selected optical frequencies. A high-temperature gas cell was used for laboratory evaluation of the NO sensor performance. A noise-equivalent sensitivity ($1\sigma$) of $\sim 100\,\mathrm{ppb} \times \mathrm{m}/\sqrt{\mathrm{Hz}}$ at room temperature and $\sim 200\,\mathrm{ppb} \times \mathrm{m}/\sqrt{\mathrm{Hz}}$ at 630 K was achieved by measuring the NO R(6.5) absorption doublet at 1900.075 $\mathrm{cm}^{-1}$.

**PACS** 42.62.Fi; 07.07.Df; 42.55.Px

## 1 Introduction

Quantum cascade lasers (QCLs) have proved to be robust light spectroscopic sources for mid-infrared (mid-IR) spectroscopic applications [1, 2]. QCL-based trace-gas sensors utilizing different detection schemes are capable of quantifying optical absorbance down to $10^{-9}\,\mathrm{cm}^{-1}$ in the mid-IR fingerprint region (fundamental molecular absorption bands) [3]. Pulsed QCLs have the advantage of operating at temperatures accessible with thermoelectric cooling. This feature makes them suitable for applications which require compact, sensitive, liquid-nitrogen-free spectroscopic instrumentation. In contrast to continuous-wave QCLs, the line width of lasers operated in a pulsed mode is broadened due to thermal chirping. However, for applications which do not require ultra-high selectivity, e.g. concentration measurements with strongly pressure-broadened spectroscopic features or measurements at low pressure using well-isolated absorption lines, a pulsed QCL is an adequate mid-IR radiation source.

✉ Fax: +1-713-348-5686, E-mail: gerardw@rice.edu

Detection of nitric oxide (NO) is important in many applications that include industrial emission and process monitoring [4, 5], atmospheric research [6, 7], and medical diagnostics [8, 9]. In recent years stricter regulatory limits for the maximum allowable concentrations of toxic pollutants in industrial exhaust gases were imposed. It triggered a need for sensors capable of real-time concentration monitoring of such gases as NO or $NH_3$ at parts per million (ppm) levels to ensure regulatory compliance. An instrument suitable for direct in situ spectroscopic analysis of industrial exhaust gases must address specific environmental challenges including atmospheric analyte gas pressure, strong non-selective absorption by soot particles, high temperature, and overlapping absorption lines of different gas species.

In this work we present the development and performance evaluation of an advanced NO sensor utilizing a thermoelectrically cooled, pulsed QCL. The laser operating at $\sim 5.26\,\mu\mathrm{m}$ ($\sim 1900\,\mathrm{cm}^{-1}$) allows the analysis of NO concentrations via the strong and quasi-interference-free absorption doublet R(6.5) at 1900.075 $\mathrm{cm}^{-1}$. Since spectral data acquisition techniques developed for cw near-infrared lasers [10, 11] are not applicable to pulsed QCLs, we report a new method of spectral manipulation and data processing.

## 2 Experimental details

### 2.1 *Methodology*

In a petrochemical plant the NO concentration levels have to be monitored in large-diameter ($\sim$ 2-m) exhaust ducts containing hot gases with a high fluctuating particulate content. The detection system should permit concentration measurements in the presence of potentially occurring turbulent optical density fluctuations and spectrally non-selective variable absorption. This can be done by applying a fast wavelength scan [11] so that spectrally non-selective beam attenuation is frozen on its time scale.

Fast wavelength tuning of a pulsed QCL is commonly performed by applying a variable sub-threshold current (usually using a sawtooth waveform) [12]. The maximum power which can be dissipated within the QCL structure as well as the laser driver electronics limit the repetition rate of the

laser injection current pulses. Thus, reducing the time span of an applied sub-threshold current ramp may result in spectrally too sparse data points insufficient for a proper spectral analysis. To minimize the number of pulses within a wavelength scan while maintaining the analytical ability of the spectrometric sensor, the data should be acquired at precisely selected optical frequencies. The absorption coefficient $\alpha(\nu)$ of a multi-species mixture at the optical frequency $\nu_k$ can be decomposed as

$$\alpha(\nu_k) = \sum_{i=1}^{n} c_i f_i(\nu_k) + b, k = 1, \ldots, m, \quad (1)$$

where $n$ is the number of species, $m$ is the number of points acquired within the scan, $f_i(\nu)$ is the absorption coefficient of the $i$th species at unity concentration, and $b$ represents the spectrally non-selective absorption. The minimum number of data points in a single scan required for the system (1) to have a unique solution is $m = n + 1$. If $m > n + 1$, $c_i$ are determined by means of multi-dimensional linear regression of $\alpha(\nu_k)$ data. The accuracy of the retrieved concentrations depends on the selection of $\nu_k$. The optimum $n$ spectral points to perform such measurements should be located at such frequencies that vectors $[f_1(\nu_1), f_2(\nu_1), \ldots, f_n(\nu_1)]$, $[f_1(\nu_2), f_2(\nu_2), \ldots, f_n(\nu_2)]$, $[f_1(\nu_n), f_2(\nu_n), \ldots, f_n(\nu_n)]$ form a closest-to-orthogonal set:

$$\sum_{k=1}^{n} f_i(\nu_k) f_j(\nu_k) = \begin{vmatrix} \max, & i = j \\ \min, & i \neq j \end{vmatrix} \quad (2)$$

In the case of narrow non-overlapping absorption lines, this criterion means that the optimum spectral sampling points are located at the maxima of the lines, plus one $(n + 1)$th point aside to determine the $b$ value in Eq. (1).

A pulsed QCL will generate the pulses only at optical frequencies $\nu_k$ if a properly shaped waveform of the laser sub-threshold current is applied [13]. The resulting scan consists of a minimum number of sequential laser pulses with individually pre-set laser frequency positions determined by the levels of the sub-threshold current pedestals, which is schematically shown in Fig. 1. Practical implementation of this approach for a particular goal of NO quantification in the industrial exhaust gases is described below.

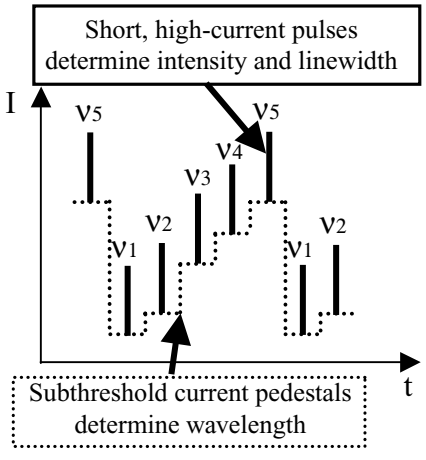


**FIGURE 1** Schematic of the laser current waveform used for rapid laser frequency scanning

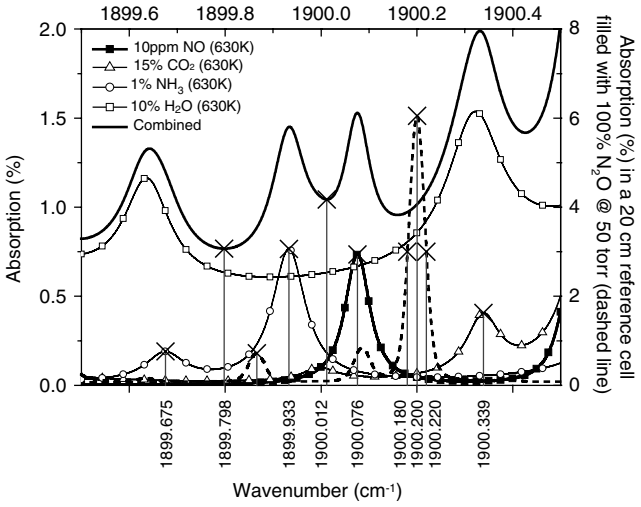


**FIGURE 2** Absorption spectra of NO, $CO_2$, $NH_3$, and $H_2O$ at atmospheric pressure and 630 K and $N_2O$ at 50 torr and room temperature at 1900 $cm^{-1}$ simulated using the HITRAN 2000 database

### 2.2 *Selection of optimum spectral sampling points*

Figure 2 shows NO, $CO_2$, $NH_3$, and $H_2O$ spectra at atmospheric pressure simulated for the expected composition and temperature (630 K) of the industrial exhaust gas using the HITRAN 2000 database [14]. This target spectral region was chosen for NO measurements considering minimum spectral interference by different exhaust gases and the strongest NO spectroscopic feature. The NO doublet R(6.5e) and R(6.5f) at $\sim 1900.075\,cm^{-1}$ was selected as the most suitable for this study [15]. Figure 2 also includes the $N_2O$ spectrum at reduced pressure (50 torr), which contains several absorption lines in this region and serves as a convenient reference for sensor-system evaluation and optical frequency control. According to the criterion of Eq. (2), the frequency positions projected on the $x$ axis in Fig. 2 were determined to be close-to-optimum for a multi-species spectrum measurement using the minimum number of points within a single frequency scan. The spectral data acquired at the wavelengths within the strongest $N_2O$ absorption line will be used for monitoring the laser frequency drift due to instabilities of the QCL temperature. These data can also be used as a feedback for active control of the QCL temperature.

### 2.3 *NO sensor configuration*

Figure 3 depicts the gas-sensor architecture. A thermoelectrically cooled pulsed distributed-feedback QCL was placed inside a vacuum-tight housing. The laser wavelength can be tuned from 1905 to 1899 $cm^{-1}$ by varying the temperature of the QCL chip from $-35$ to $+10^{\circ}C$. Fast frequency scanning of the QCL was performed using sub-threshold laser current modulation at a fixed temperature of the QCL heat sink [1, 12]. Twenty-five-nanosecond-long injection

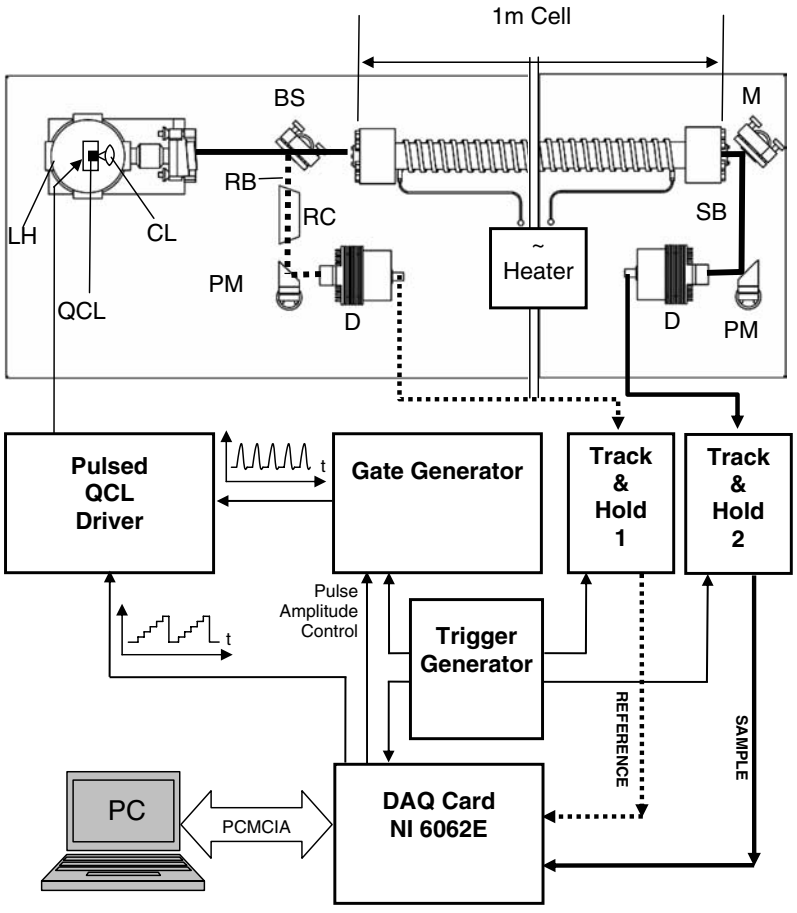


**FIGURE 3** Schematic diagram of pulsed QCL-based spectroscopic sensor. *QCL* – quantum cascade laser chip; *LH* – laser housing; *CL* – collimating lens; *SB* – sample beam; *RB* – reference beam; *M* – mirror; *BS* – beam splitter; *PM* – off-axis parabolic mirror; *RC* – reference cell; *D* – photodetector

current pulses were supplied to the laser at a repetition rate of 240 kHz. The maximum repetition rate of the laser pulses was primarily limited by the maximum sampling rate of the data-acquisition electronics. The measurement method uses dual-channel (sample and reference) data acquisition [16]. The reference channel is used for signal normalization to the optical energy of each laser pulse to minimize the influence of $\sim 5\%$ pulse-to-pulse QCL fluctuations. This technique significantly improves the signal-to-noise ratio (SNR) of the measured absorption data acquired by means of the pulsed QCL-based system. After collimation by an anti-reflection-coated ZnSe aspherical lens with 3-mm focal length and 6-mm diameter located inside the laser housing, the laser beam is divided into sample and reference beams in a $\sim 50/50$ ratio using a ZnSe beam splitter as shown in Fig. 3. The sample beam passes through a gas cell with an optical path length of 1 m. To simulate high-temperature conditions in a real industrial exhaust duct the gas cell was equipped with resistive heaters capable of elevating the gas temperature to 810 K. Upon exiting the gas cell the QCL radiation is focused onto a fast (50-MHz bandwidth) photovoltaic Hg–Cd–Zn–Te detector (Vigo Systems Ltd., model PDI-2TE-6) using an off-axis parabolic mirror. The reference beam is directed through the reference cell and is subsequently focused onto a second detector of the same kind. Fast track-and-hold (T&H) electronics with a 350-MHz sampling bandwidth and 125-MHz maximum sampling rate (Analog Devices, model AD9101) is implemented for capturing the peak optical intensity of the detected sample and reference laser pulses. T&H electronics operate as an analog buffer, which captures and retains an input voltage value as long as necessary for successive digitization with an analog-to-digital converter. In this work data acquisition and processing were performed by a laptop computer equipped with a 500-Ksample/s PCMCIA data-acquisition card (DAQ card) (National Instruments, model DAQ 6062E). Two analog outputs of the data-acquisition card are used for generation of the laser control signals: a sub-threshold current waveform for frequency scanning and a current pulse amplitude modulation waveform for the laser power control within a wavelength scan [17]. The application of the multi-function DAQ card significantly increases the flexibility of the sensor system, allowing it to be programmed to perform either conventional wavelength scans using a lower-frequency saw-tooth waveform with a large number of laser pulses or a rapid scan as described in this work. The overall system timing is performed by an external pulse generator (Stanford Research Systems, model DG535).

### 2.4 *Spectral calibration of the system*

The wavelength tuning of a QCL using sub-threshold current modulation occurs as a result of Joule heating of the QCL structure. Due to a temperature rise, the refractive index of the active region changes, which results in wavelength tuning of the emitted radiation. If low-frequency

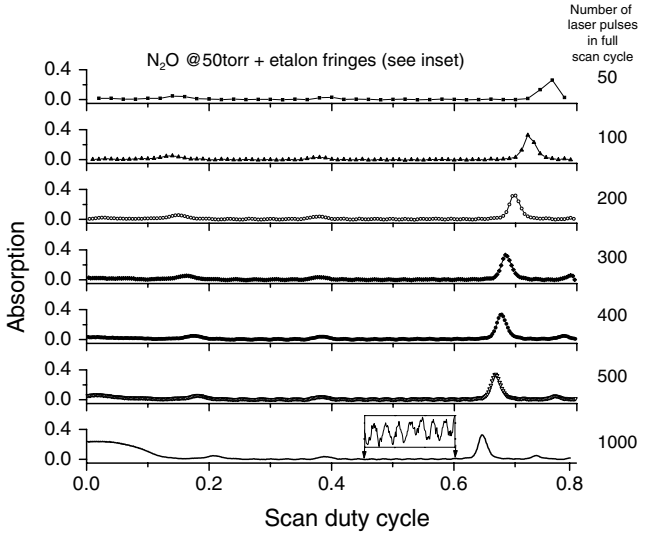


**FIGURE 4** Spectra of pure $N_2O$ at 50 torr recorded with different scan speeds. The QCL repetition rate of 240 kHz remains the same for all acquired spectra

waveforms (of the order of $10^2$ Hz) are applied the process can easily follow the control signals and the system inertia can be neglected. Thus, a slow scan with a large number of laser pulses is relatively easy to perform and to calibrate using for example an etalon fringe pattern as a relative wavelength standard. The situation changes in the case of rapid wavelength scanning performed at frequencies of several kilohertz. Transient effects caused by the thermal inertia of the laser chip become strongly pronounced. It is illustrated by Fig. 4, which shows several spectra of pure $N_2O$ at 50 torr recorded using a common saw-tooth waveform for sub-threshold current modulation at different frequencies. The waveforms were synthesized by the DAQ card maintaining a duty cycle and an amplitude (and thus an average power dissipated within the laser structure) at constant levels. Despite the smaller number of laser pulses, the scanning range decreases significantly for faster scans. The largest influence of the thermal inertia is visible at the beginning and at the end of the scan, while the center frequency remains almost unchanged. The regular structure in the spectra with a higher number of data points is a fringe pattern from the etalon, which was introduced into the laser beam simultaneously with the gas cell to obtain a high-precision spectral reference. This set of spectra also demonstrates that the resolution of the fast scans with a small number of spectral data points is insufficient to perform calibration using a comparison with the same etalon reference fringe pattern. Thus, for rapid-scan measurements a special wavelength-calibration process was developed.

Wavelength tuning of a QCL can be performed by varying the laser heat-sink temperature. This is an alternative to sub-threshold current modulation. Thermal tuning is linear over a wide range of temperature variation and independent of the laser sub-threshold current amplitude. For the laser used in this work the tuning coefficient was measured to be $\mathrm{d}\nu/\mathrm{d}T = 0.15\,\mathrm{cm}^{-1}/\mathrm{K}$. We used this laser property to perform wavelength calibration of a rapid scan. Scanning the laser heat-sink temperature with a resolution of 0.04 K and scanning rates on the order of $10^{-2}$ K/min, rapid wavelength scans were implemented for each point of the temperature scan and the resulting absorption spectrum was calculated and stored in the computer memory for further processing. Subsequently, the stored data points could be analyzed as a function of the heat-sink temperature. For each sub-threshold current level a corresponding spectrum recorded by means of a temperature scan is extracted. Such spectra can be calibrated in a wavelength scale by comparing them with a reliable database. In this manner for each point on the temperature scale a wavelength associated with each pedestal of the sub-threshold current ramp can be determined. Such a set of wavelengths at a given laser heat-sink temperature fully characterizes the applied rapid-scan waveform. Figure 5a shows a set of spectra resulting from such a dataset acquired for a rapid scan with equidistant sub-threshold current pedestals. Each scan contained 15 laser pulses (13 points for the actual scan and two points for detector 'zero' retrieval and thermal relaxation of the laser) at a repetition rate of 240 kHz; hence, its duration was 62.5 $\mu$s. The resulting wavelength-calibration curve of the applied sub-threshold current waveform is shown in Fig. 5b. For the first three points of the actual ramp in the control signal

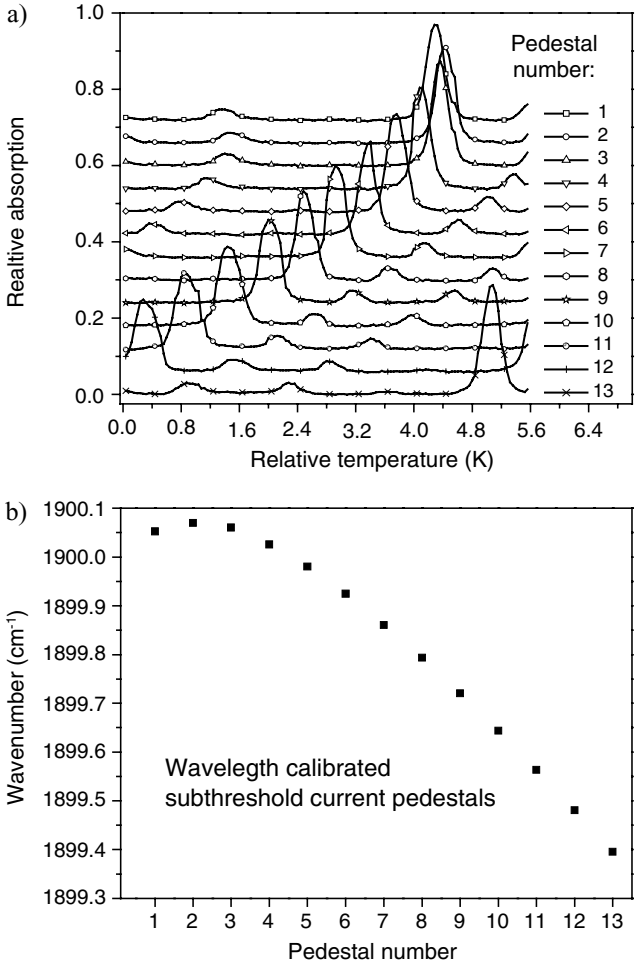


**FIGURE 5** **a** Absorption spectra recorded for each sub-threshold current pedestal in the fast laser wavelength scan as a function of the laser heat-sink temperature. **b** Wavelength calibration derived from the thermal QCL wavelength scan depicted in (**a**) for equidistant sub-threshold current pedestals

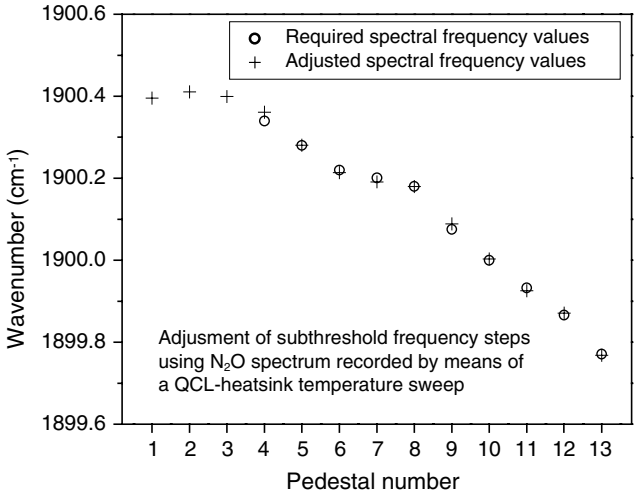


**FIGURE 6** Values of the required set of laser wavelengths plotted together with values obtained in the calibration process for the designed rapid scan

the previously mentioned thermal transient effects are clearly visible as a flattened part in the wavelength-calibration plot. This demonstrates the limited response time of the sensor to the sub-threshold current wavelength tuning process. Due to this limitation, there is no simple linear relation between the pedestal amplitude and the resulting wavelength. Therefore, the wavelength-optimization process has to be performed incrementally by applying small-amplitude corrections individually to each pedestal and subsequently calibrating the scan as described above. The results of such a calibration process are depicted in Fig. 6. The circles in the graph represent the required wavelength (see Fig. 2) and the crosses depict the wavelength resulting from the optimization process. A calibration accuracy of $\pm 0.015\,\mathrm{cm}^{-1}$ was achieved.

In all our measurements the laser power was controlled and maintained nearly constant within the scan (see [17] for details). Both the sub-threshold current waveform resulting in the desired optical frequency scan and the laser power monitored by the reference channel during a single scan cycle are shown in Fig. 7.

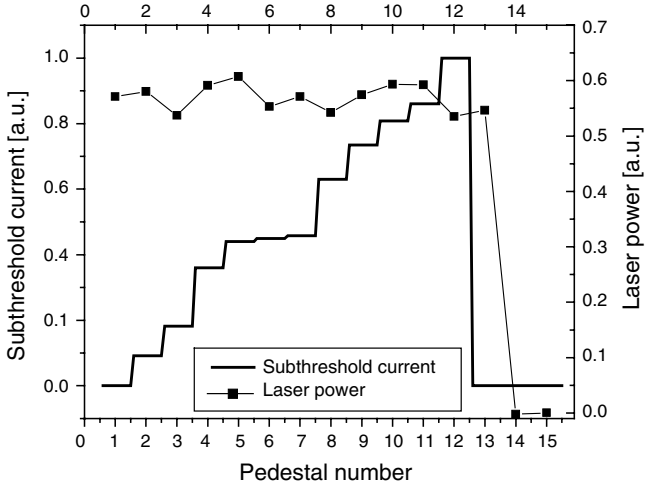


**FIGURE 7** An example of a sub-threshold current waveform applied to the QCL plotted together with equalized laser pulses' peak power monitored during a single scan

### 2.5 *Measurement results*

*2.5.1 Spectral measurements.* The sensor performance was evaluated by recording spectra of pure $N_2O$ at 50 torr and of a 10-ppm NO in $N_2$ mixture at 760 torr in a 1-m-long gas cell. The measurements were performed using a calibrated rapid scan and a conventional scan (400 points). Both spectra were acquired at the same laser power level to insure identical laser operating conditions and permit a direct comparison of the results. The absorption spectra were calculated by averaging 1000 scans for both methods. The resulting spectra of the gas samples at two different temperatures, room temperature ($\sim 296\,\mathrm{K}$) and $\sim 630\,\mathrm{K}$, are plotted together with appropriate simulations in Figs. 8 and 9, respectively. Agreement of the absorption data measured using both the rapid and conventional scans was observed in all cases. This confirms the validity of the frequency calibration of the rapid wavelength scan. All the room-temperature measurements also show a consistency with the spectra simulated using the HITRAN

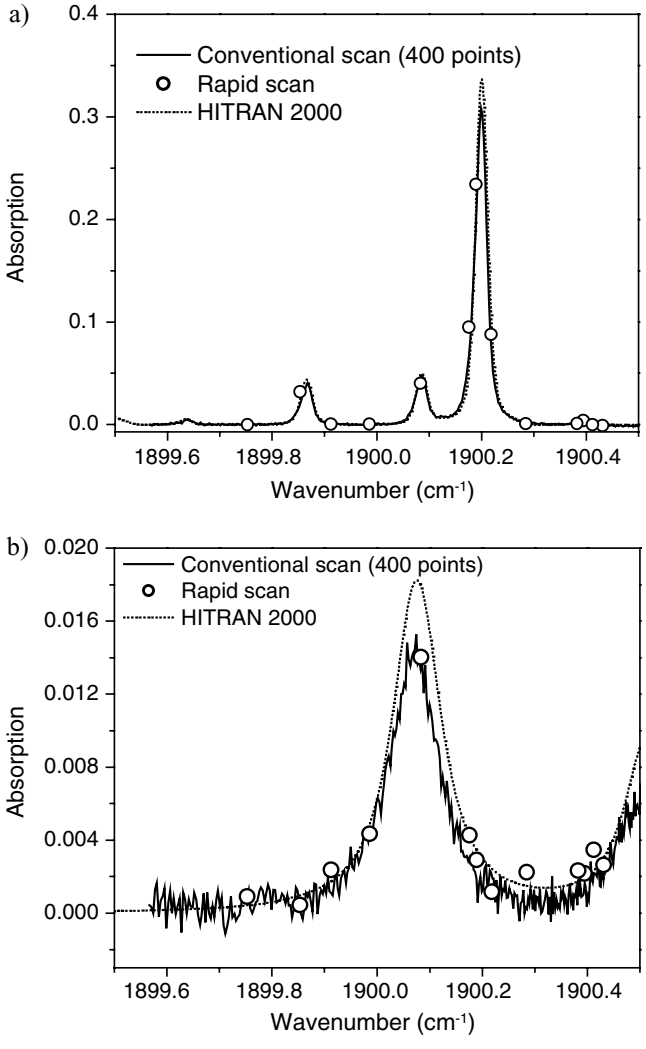


**FIGURE 8** Spectra of pure $N_2O$ at 50 torr (**a**) and 10-ppm NO in $N_2$ mixture at 760 torr (**b**), recorded at room temperature using both rapid-scan and conventional scan methods. Both graphs include a simulation calculated using a HITRAN 2000 spectrum convoluted with a Gaussian function ($0.035\,\mathrm{cm}^{-1}$ FWHM)

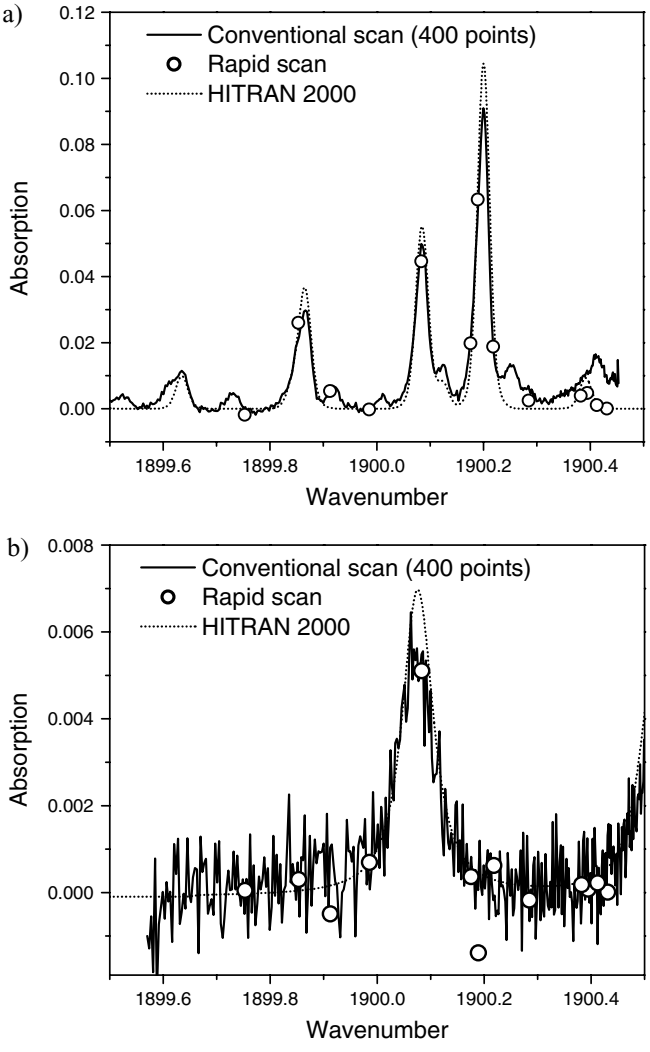


**FIGURE 9** Spectra of pure $N_2O$ at 50 torr (**a**) and 10-ppm NO in $N_2$ mixture at 760 torr (**b**), recorded at 630 K using both rapid-scan and conventional scan methods. Both graphs include a simulation calculated using a HITRAN 2000 spectrum convoluted with a Gaussian function (0.035 $cm^{-1}$ FWHM)

2000 database. The HITRAN high-resolution spectrum was convoluted with a Gaussian function (0.035 $cm^{-1}$ FWHM), which simulates the influence of the finite laser line width. At elevated temperatures (630 K) the simulated spectrum of pure $N_2O$ does not include all of the weaker absorption lines that are observed in the measured data. For the 10-ppm NO mixture we observed agreement between the measured and simulated spectra. The single-point standard deviation calculated using the residual of the conventional scan measurements is on the level of $\sim 6 \times 10^{-4}$ for 1000 averages. This yields an estimated single-point noise-equivalent sensitivity for NO of $\sim 0.4$ ppm at room temperature and $\sim 0.9$ ppm at 630 K.

*2.5.2 Baseline fluctuations.* Application of the rapid scan has a significant advantage in the effective elimination of $1/f$ noise. Sources of this noise are usually difficult to locate and suppress, which makes the minimization of its influence an important issue. The basic sources of the $1/f$ noise include mechanical vibrations of the optical system and electronic

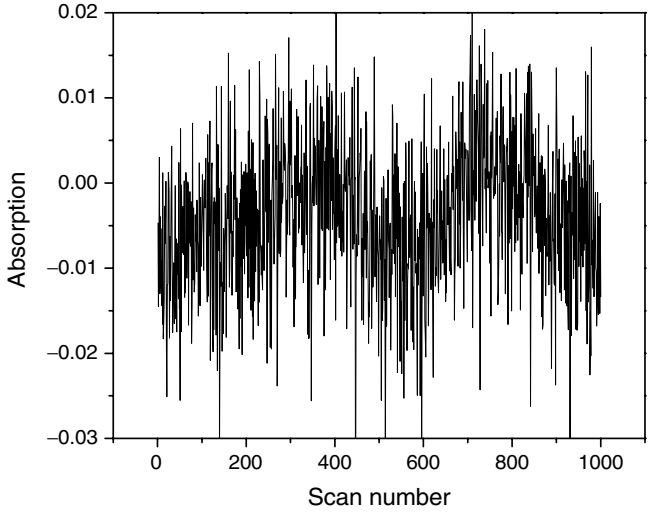


**FIGURE 10** Fluctuations of the mean value calculated for each spectrum from a set of 1000 continuously recorded rapid scans

noise in the detection system. In spectroscopic applications the slower components of noise occur usually as baseline fluctuations of the measured spectra, which tend to deteriorate the instrument sensitivity. Rapid wavelength scanning is aimed to make the sensor immune to fluctuations of non-selective absorption (e.g. due to soot particles). This technique also allows the fluctuations of the baseline within a single scan to be considered as a simple change of a constant value $b$ (Eq. (1)). Such an assumption significantly simplifies processing of the acquired data. To visualize an effect of suppression of baseline fluctuations, a set of 1000 continuously acquired rapid scans of pure $N_2$ was analyzed. The mean apparent absorption value was calculated for each scan. Figure 10 shows variations of the calculated absorption values. This plot depicts fluctuations of a flat baseline $b$ for 62.5 ms for the entire acquisition period. In comparison to the conventional 400-point scan, which lasts $\sim 1.7$ ms, the rapid scan consisting of 13 effective points acquired within $\sim 55\,\mu$s is automatically immune to 30 times faster noise components. With the assumption that the system is insensitive to the noise components with a period 10 times longer than the spectral scan, the upper-frequency limit would be 58 Hz and 1.8 kHz for conventional and rapid scans, respectively. Hence, the low-frequency noise can affect the conventional scans. This effect can be seen in the $N_2O$ measurement shown in Fig. 9a. Such a baseline drift is visible in the spectrum measured with the conventional frequency scan from 1900.03 to 1900.45 $cm^{-1}$, while the data acquired using a rapid scan do not show baseline distortion, and the measured absorption is in good agreement with the simulated spectrum.

An analysis of the averaging process efficiency was performed for a quantitative evaluation of the baseline-drift influence using both rapid and conventional scans. A large number $X$ of spectra were recorded for this purpose. Each single scan in the acquired spectra sets was baseline $b$ corrected. A mean value of a two-sample variance,

$$\langle \sigma_k^2(N) \rangle = \frac{1}{2(n-1)} \sum_{i=1}^{n-1} [M_{k,i+1}(N) - M_{k,i}(N)]^2,$$

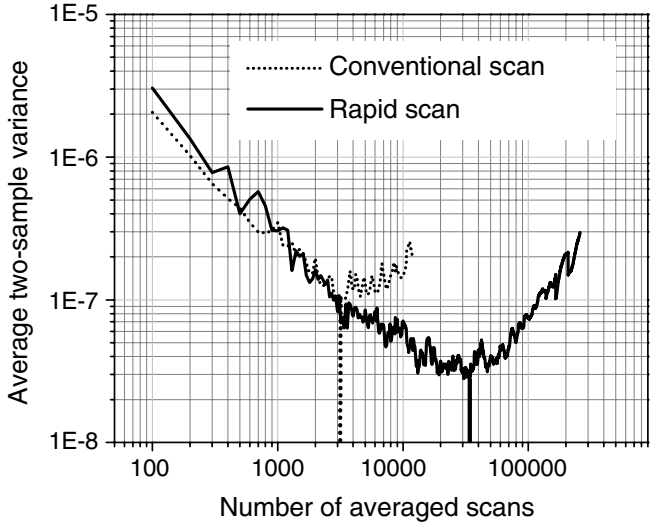


**FIGURE 11** Two-sample variance averaged within the entire spectrum as a function of the number of averaged scans

as a function of the number of averaged scans $N$ was calculated for each point of the spectrum $k$ using $n = \lfloor X/N \rfloor$ subsets of the acquired data points. $M$ in the above expression denotes a mean value of the $s$th data point sub-set calculated for the $k$th point of the spectrum:

$$M_{k,s}(N) = \frac{1}{N} \sum_{i=1+(s-1)N}^{sN} \alpha_{i(\nu_k)} \; ; \; s = 1, \ldots, n.$$

A variation of this number within the entire scan reflects the actual baseline fluctuation, which is a useful parameter for the evaluation of its influence on the averaging process. For both rapid and conventional scan measurements the value of the two-sample variance averaged over $K$ points of the analyzed spectrum

$$\frac{1}{K} \sum_{k=1}^{K} \left\langle \sigma_k^2(N) \right\rangle$$

is plotted in Fig. 11. The first linear parts of the curves show that the system in both cases is dominated by the same level of white noise. However, for a conventional scan, due to the higher baseline drift (low-frequency noise), increasing the number of averaged spectra beyond $\sim 3000$ becomes inefficient. The same effect for a rapid scan occurs at one order of magnitude higher number of averaged spectra, which allows us to achieve a $\sim 2$ times lower single-point noise-equivalent detection limit. This demonstrates the ability of the rapid-scan method to be efficient for gas-monitoring applications in harsh and noisy measurement environments.

*2.5.3 Real-time concentration measurements.* Data acquisition and processing is realized using a LabView-based control platform. Calculation of the component concentration coefficients from Eq. (1) is performed by means of a least-squares linear fitting algorithm. Pre-acquired spectra of reference gas mixture were used as component functions $f_i(\nu_k)$. This eliminates the need of taking into account an instrument function of the pulsed QCL-based system, which is necessary to consider during the synthesis of a spectrum using a spectroscopic database. Furthermore, this method is also immune to eventual discrepancies between a simulated and a measured spectrum as shown in Fig. 9.

Wavelength stability is an important issue, since it influences the quality of the rapid-scan measurements. To monitor the laser wavelength a 10-cm reference cell filled with $N_2O$ at 50 torr located in the reference channel was used. The $N_2O$ concentration was adjusted to the level at which only the strongest line within the operating range was above the detection limit of the sensor system. This prevents interference with other spectral features. The spectral points of the rapid scan located on the $N_2O$ line at 1900.02 $cm^{-1}$ were used for laser frequency monitoring. The sensor described in this work was not equipped with active feedback control of the laser wavelength. However, to insure the measurement accuracy, data acquisition was only performed when the monitored laser frequency had precisely the pre-selected value.

The system performance was evaluated by measurements of NO concentration in the calibrated mixture. An initially evacuated gas cell was sequentially filled with 760 torr of zero gas (high-purity-grade $N_2$) and 10-ppm NO mixture. For the single-component mixture the fitting of a basic function $\alpha(\nu_k) = c_1 f_1(\nu_k) + b$ was implemented, where $f_1(\nu_k)$ was interpolated using a pre-acquired spectrum of a NO calibration mixture for a known concentration $C_{\text{ref}}$. Figure 12a shows a time series of the measured concentration calculated as $C_{\text{NO}} = c_1 C_{\text{ref}}$. For calculation of each data point in this plot, a spectrum resulting from averaging of 1000 scans was used. Statistical analysis shows $1\sigma$ scattering of the data points at the level of 0.39 ppm, which is in good agreement with the single-point noise-equivalent sensitivity estimated on the basis of the conventional scan measurement shown in Fig. 8. Hence, the sensor is capable of performing real-time concentration monitoring with a 62.5-ms resolution. The NO sensitivity at 296 K is $\sim 100$ ppb $\times$ m/$\sqrt{\text{Hz}}$ when normalized to path length and acquisition time. Results of similar measurements performed at 630 K are presented in Fig. 12b. A NO mixture level of $\sim 3$ ppm was achieved by dilution of the 10-ppm NO calibration mixture by the zero gas ($N_2$). The $1\sigma$ scattering of data points at the 0.81-ppm level is also in agreement with the previous approximation and results in a normalized sensitivity of $\sim 200$ ppb $\times$ m/$\sqrt{\text{Hz}}$.

*2.5.4 Influence of the laser power on the sensor detection limit.* All the measurements were performed at close-to-threshold injection current of the QCL in order to achieve a relatively small line width, which allows more accurate analysis of the system behavior. However, increasing the laser power will improve the sensitivity, which is primarily limited by electronic noise of the detection system. A conventional scan spectrum of a 10-ppm NO mixture at 760 torr depicted in Fig. 13a was taken to demonstrate the improvement of sensor performance by using a two times higher laser power. Since the measurement was carried out at atmospheric pressure, laser line-width broadening has only a minor effect on the shape of the NO spectrum. However, the residual noise is reduced by $\sim 35\%$, which as demonstrated above represents a similar reduction of the noise level for a rapid scan. In this manner we can estimate a NO sensitivity of

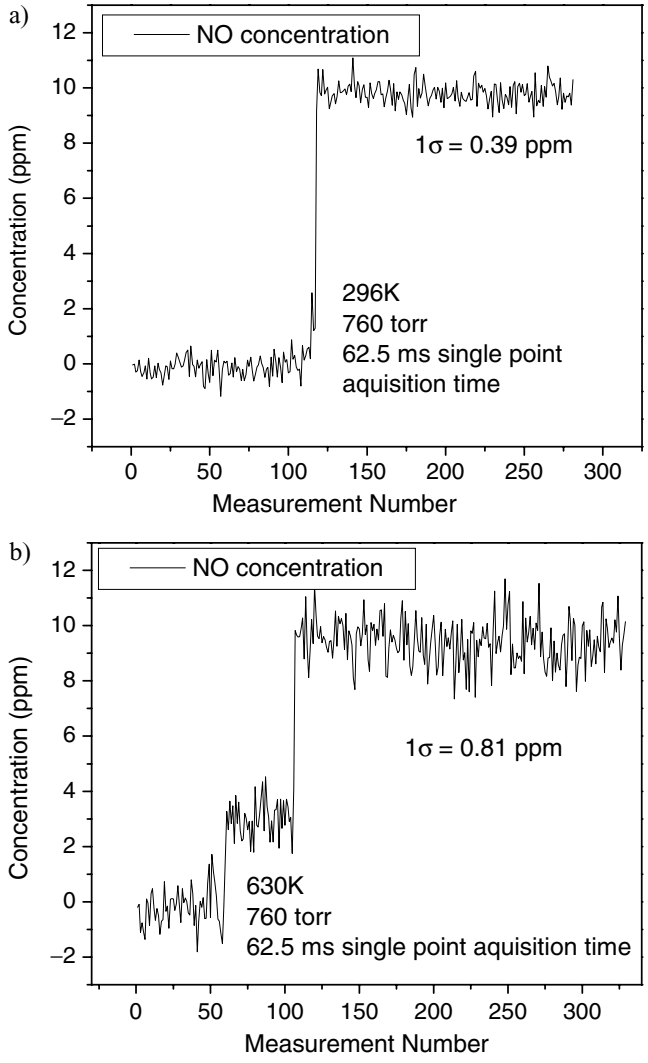


**FIGURE 12** Concentration measurements of NO performed at **a** room temperature and **b** 630 K

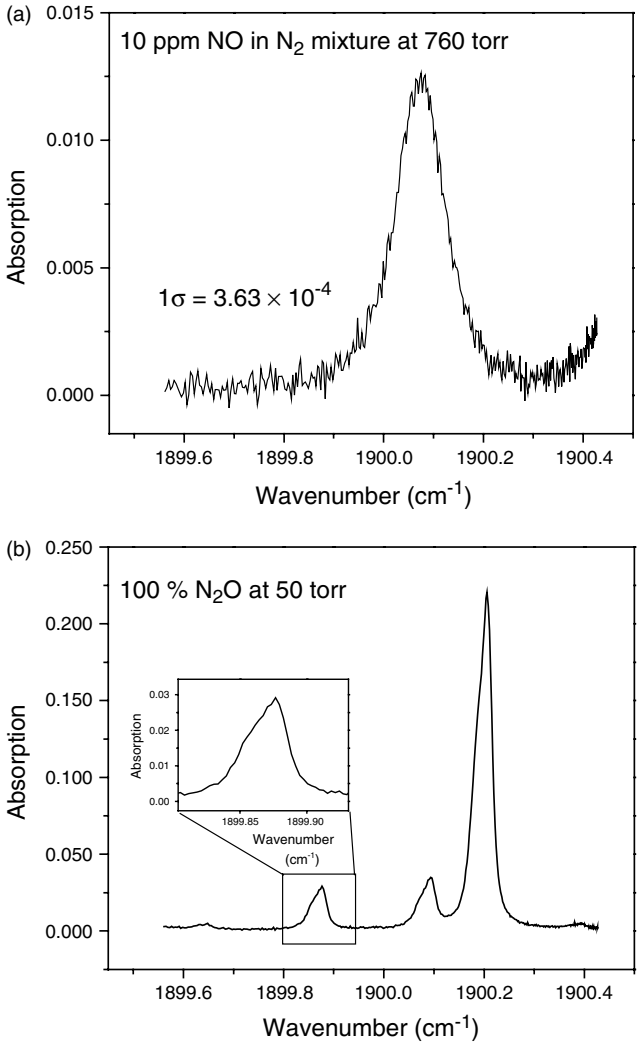


**FIGURE 13** Spectra of **a** 10-ppm NO in $N_2$ mixture at 760 torr and **b** pure $N_2O$ at 50 torr recorded at room temperature using conventional scan method and an increased laser power (∼ 2 times) in comparison to previous measurements depicted in Fig. 8

∼ 70 ppb × m/$\sqrt{\text{Hz}}$ at 296 K and of ∼ 150 ppb × m/$\sqrt{\text{Hz}}$ at 630 K. Figure 13b depicts a $N_2O$ spectrum at a pressure of 50 torr recorded using the same elevated laser power. This spectrum clearly shows the influence of an asymmetrically broadened laser line on spectral measurements of gas samples at reduced pressure (see inset in Fig. 13b).

*2.5.5 Multi-species measurement.* To demonstrate the feasibility of multi-species concentration measurements the system was tested using a gas mixture containing both NO and $CO_2$. The gas sample was prepared by mixing pure $CO_2$ with the 10-ppm NO-doped $N_2$ in a ratio of 1:5. The mixing process was performed in the gas cell using the pressure-meter readings to determine the mixing ratio within an accuracy of ∼ 5%. The resulting concentrations of NO and $CO_2$ in the gas mixture are 8 ppm and 20%, respectively. The fitting process of the function $\alpha(\nu_k) = c_1 f_1(\nu_k) + c_2 f_2(\nu_k) + b$ was implemented for two-species concentration measurement. Reference spectra were recorded using 10-ppm NO in $N_2$ mixture and 100% $CO_2$, respectively, to determine the component functions $f_1$ and $f_2$. The data processing of a set of 1000 rapid spectra acquired within 62.5 ms resulted in the measured concentrations of ∼ 7 ppm for NO and ∼ 13% for $CO_2$. The mixture absorption spectra obtained by means of the rapid-scan averaging process, the composite spectrum calculated using coefficients derived by the fitting routine, and the corresponding conventional scan spectrum are shown in Fig. 14. This experiment demonstrates the multi-species monitoring capability of the sensor. We found a good correlation of the measured NO concentration with the value calculated from the dilution ratio. The presence of significant (∼ 9%) uniform background absorption of the pure $CO_2$ at the elevated temperature was observed, which was not predicted by the HITRAN simulations. The shape of the $CO_2$ spectral envelope was in good agreement with the simulated data. Such a uniform shift of the spectrum becomes a dominating change due to concentration variations. However, the sensor, which is designed to omit variations of a flat baseline $b$, is primarily sensitive to changes in the spectral envelope shape. Thus, the accuracy of the $CO_2$ concentration measurement, which has relatively weak ro-vibrational transitions within the measured

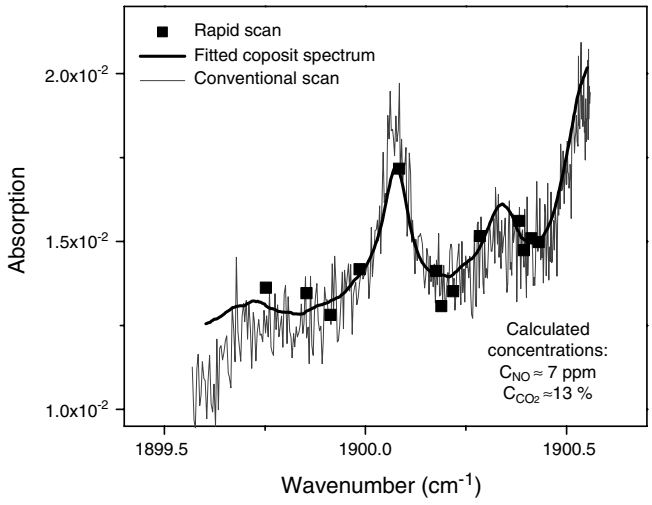


**FIGURE 14** Absorption measurements of a two-component mixture ($\sim$ 8-ppm NO and $\sim$ 20% $CO_2$) performed using a rapid-scan spectrum and a fitting algorithm for concentration retrieval. A measurement by means of the conventional scan method is plotted for comparison

spectral range, is sufficient for monitoring this species at the percent level.

## 3 Summary

A NO trace-gas sensor based on a mid-IR pulsed QCL as spectroscopic source and employing an original method of rapid wavelength scanning has been developed. The system is dedicated to perform detection of trace gases at elevated temperatures in the harsh environment of industrial combustion exhaust systems. The laboratory experiments with a 1-m high-temperature gas cell demonstrated a detection limit of $\sim 200\,\mathrm{ppb} \times \mathrm{m}/\sqrt{\mathrm{Hz}}$ ($1\sigma$) for the NO species at 630 K, which can be further improved by optimizing the laser power level. Due to the rejection of low-frequency noise components up to 1.8 kHz the described gas-sensor system is able to minimize the influence of non-selective absorption fluctuations and other sources of noise, which can exhibit themselves as baseline distortions. The applicability of the developed measurement and data-processing methods to multi-species concentration monitoring was demonstrated.

Further system improvements can be implemented to increase system performance and reliability. One of the key factors required for appropriate system operation is QCL wavelength stability. Thus, an active feedback control of the QCL operating temperature should be applied for precise wavelength stabilization by means of a reference gas cell. Significant improvement of system performance can also be obtained by development of high-speed control and detection electronics and system integration.

**ACKNOWLEDGEMENTS** The authors wish to thank Prof. Robert F. Curl, Trevor Knittel of Analytical Specialties, Inc., and J.D. Tate of Dow Chemical for very useful discussions. The authors acknowledge financial support from the Texas Advanced Technology Program and the Office of Naval Research via a sub-award from Texas AM University.

## REFERENCES

1 A.A. Kosterev, F.K. Tittel, IEEE J. Quantum Electron. (Spec. Issue Quantum Cascade Lasers) **38**, 582 (2002)
2 D. Weidmann, G. Wysocki, C. Oppenheimer, F.K. Tittel, Appl. Phys. B **80**, 255 (2005). DOI 10.1007/s00340-004-1639-7
3 F.K. Tittel, D. Richter, A. Fried, in *Solid-State Mid-Infrared Laser Sources*, ed. by I.T. Sorokina, K.L. Vodopyanov (Top. Appl. Phys. **89**) (Springer, Berlin Heidelberg New York, 2003), pp. 445–510
4 H. Gupta, L.-S. Fan, Ind. Eng. Chem. Res. **42**, 2536 (2003)
5 G.R. Price, K.K. Botros, G.M. Goldin, J. Eng. Gas Turbines Power **124**, 276 (2002)
6 D.R. Fitz, K. Bumiller, A. Lashgari, Atmos. Environ. **37**(Suppl. 2), S119 (2003)
7 C. Stroud, S. Madronich, E. Atlas, B. Ridley, F. Flocke, A. Weinheimer, B. Talbot, A. Fried, B. Wert, R. Shetter, B. Lefer, M. Coffey, B. Heikes, D. Blake, Atmos. Environ. **37**, 3351 (2003)
8 P.E. Silkoff, M. Caramori, L. Tremblay, P. McClean, C. Chaparro, S. Kesten, M. Hutcheon, A.S. Slutsky, N. Zamel, S. Keshavjee, Am. J. Respir. Crit. Care Med. **157**, 1822 (1998)
9 S.A. Kharitonov, P.J. Barnes, Am. J. Respir. Crit. Care Med. **163**, 1693 (2001)
10 T. Fernholz, H. Teichert, V. Ebert, Appl. Phys. B **75**, 229 (2002)
11 H. Teichert, T. Fernholz, V. Ebert, Appl. Opt. **42**, 2043 (2003)
12 K. Namjou, S. Cai, E.A. Whittaker, J. Faist, C. Gmachl, F. Capasso, D.L. Sivco, A.Y. Cho, Opt. Lett. **23**, 219 (1998)
13 A.A. Kosterev, C. Roller, F.K. Tittel, in *IEEE Sensors 2003*, Toronto, Canada, 22–24 October 2003, Book of Abstracts, pp. 176–177
14 L.S. Rothman A. Barbe, D. Chris Benner, L.R. Brown, C. Camy-Peyret, M.R. Carleer, K. Chance, C. Clerbaux, V. Dana, V.M. Devi, A. Fayt, J.-M. Flaud, R.R. Gamache, A. Goldman, D. Jacquemart, K.W. Jucks, W.J. Lafferty, J.-Y. Mandin, S.T. Massie, V. Nemtchinov, D.A. Newnham, A. Perrin, C.P. Rinsland, J. Schroeder, K.M. Smith, M.A.H. Smith, K. Tang, R.A. Toth, J. Vander Auwera, P. Varanasi, K. Yoshino, J. Quantum Spectrosc. Radiat. Transfer **82**, 5 (2003)
15 S. Wehe, M. Allen, X. Liu, J. Jeffries, R. Hanson, Sensors. In *Proceedings of IEEE*, 22–24 October 2003, vol. 2, pp. 795–800
16 A.A. Kosterev, F.K. Tittel, R. Köhler, C. Gmachl, F. Capasso, D.L. Sivco, A.Y. Cho, S. Wehe, M.G. Allen, Appl. Opt. **41**, 1169 (2002)
17 G. Wysocki, M. McCurdy, S. So, D. Weidmann, C. Roller, R.F. Curl, F.K. Tittel, Appl. Opt. **43**, 6040 (2004)